ACS APPLIED MATERIALS & INTERFACES

Research Article

www.acsami.org

Green Synthesis of Anatase TiO_2 Nanocrystals with Diverse Shapes and their Exposed Facets-Dependent Photoredox Activity

Nitish Roy,[†] Yohan Park,[‡] Youngku Sohn,[‡] Kam Tong Leung,[§] and Debabrata Pradhan*[,†]

[†]Materials Science Centre, Indian Institute of Technology, Kharagpur 721 302, W.B. India

[‡]Department of Chemistry, Yeungnam University, Gyeongsan, Gyeongbuk 712-749, Korea

[§]Department of Chemistry, University of Waterloo, Waterloo N2L 3G1, Ontario Canada

Supporting Information

ABSTRACT: The exposed facets of a crystal are known to be one of the key factors to its physical, chemical and electronic properties. Herein, we demonstrate the role of amines on the controlled synthesis of TiO_2 nanocrystals (NCs) with diverse shapes and different exposed facets. The chemical, physical and electronic properties of the as-synthesized TiO_2 NCs were evaluated and their photoredox activity was tested. It was found that the intrinsic photoredox activity of TiO_2 NCs can be enhanced by controlling the chemical environment of the surface, i.e.; through morphology evolution. In particular, the rod shape TiO_2 NCs with ~25% of {101} and ~75% of {100}/{010} exposed facets show 3.7 and 3.1 times higher photocatalytic activity than that of commercial Degussa P25 TiO_2 toward the degradation of methyl orange and methylene blue, respectively. The higher activity of the rod shape TiO_2 NCs is ascribed to the facetsphilic nature of the photogenerated carriers within the NCs. The photocatalytic activity of TiO_2 NCs are found to be in the order of {101}+{100}/{010} (nanorods) > {101}+{001}+{100}/{010} (nanocuboids and nanocapsules) > {101} (nanoellipsoids) > {001} (nanosheets) providing the direct evidence of exposed facets-depended photocatalytic activity.

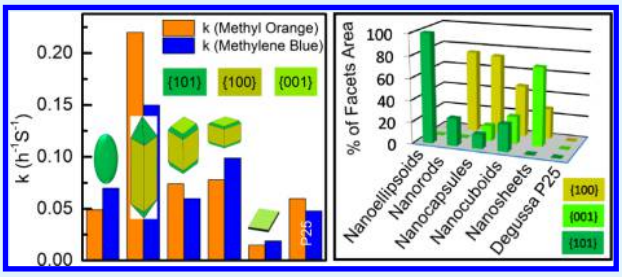

KEYWORDS: *TiO_2 nanocrystals, shape-control, growth mechanism, photocatalysis, redox activity, capping agent*

1. INTRODUCTION

Titanium dioxide (TiO_2) is one of the important oxides that finds extensive application in the field of photocatalysis,[1−4] phototovoltaics,[5,6] pigments,[7,8] and hydrogen production.[9−11] The performance in the aforementioned applications predominantly depends on the surface physicochemical properties of TiO_2 crystals, which are known to vary with its size, shape, crystal structure, and exposed facets. Therefore, it is worth it to precisely control the morphology of TiO_2 crystals and understand their growth mechanism. There are several reports on the synthesis of TiO_2 nanocrystals (NCs) using solution-based techniques such as sol−gel, reverse micelle, sonochemical, hydrothermal, and solvothermal.[12−16] The detail on the synthesis of TiO_2 nanomaterials using different techniques has been reviewed thoroughly.[17,18] The crystal shape of TiO_2 is primarily dictated by its growth direction. Under equilibrium conditions, both the natural and synthetic anatase TiO_2 crystals grow along [001] which exposes the low-energy {101} facets thereby minimizing the surface energy and increasing the crystal stability by forming truncated bipyramidal shapes. Theoretical calculation reveals that the surface energy of major exposed facets of anatase TiO_2 crystal follows the order $\gamma\{110\} > \gamma\{001\} > \gamma\{100\} > \gamma\{101\}$.[19,20] Thus, the TiO_2 crystals with high-energy exposed facets are desirable for improved photocatalysis.[21] Yang et al. successfully synthesized micron size TiO_2 crystals with {001} exposed facets using hydrofluoric (HF) acid as a morphology controlling agent.[22] Subsequently there are several recent reports on controlling the high-energy {001} and {100} exposed facets of TiO_2 crystals but all of those use HF as facets terminating agent.[20,21,23−26] HF is known to be a highly corrosive, harmful and environmentally unfriendly chemical reagent. Therefore, it is desirable to find fluorine-free process to grow TiO_2 crystals with high-energy exposed facets. There are a few recent reports on the synthesis of TiO_2 NCs with the shape of truncated tetragonal bipyramidal (and related bipyramidal shapes) and 16-faceted polyhedrons using fluorine-free process to expose high-energy facets.[27−30] In these studies, precursors such as potassium titanate nanowires and titanium isobutoxide or titanium isopropoxide, and capping agents such as carbonates ions, polyvinylpyrrolidone, and acetic acid were used to obtain TiO_2 crystals. However, there is no report on the systematic control of TiO_2 NCs shapes, their growth mechanism, and surface specific photoredox activity. Furthermore, there are growing inconsistencies of both theoretical and experimental

Received: March 13, 2014
Accepted: September 4, 2014
Published: September 4, 2014

works on the role of different exposed facets on the photocatalysis.[31−36]

In the present work, we demonstrate diethanolamine (DEA) as a powerful and major shape-controlling agent to synthesize TiO_2 NCs in the shape of ellipsoid, rod, capsule, cuboid and sheet-like with different ratios of high-energy and low-energy exposed facets. The detail growth mechanism of TiO_2 NCs with tunable ratio of high-energy and low-energy exposed facets using a green fluorine-free process is described. The physical, chemical, and electronic properties of as-synthesized TiO_2 NCs with diverse shapes are evaluated to understand the role of exposed facets for their intrinsic photoredox activity. In our previous report, we demonstrate the synergy of high-energy {001} and low-energy {101} exposed facets in the TiO_2 nanocuboids for the improved photocatalytic activity.[34] Here, we show that combination of {100}/{010} and {101} exposed facets have highest photocatalytic activity suggesting {100}/{010} facets is more active than that of {001} facets. This conclusion could be made because of the successful synthesis of TiO_2 NCs with diverse shapes and study of their photocatalytic performance.

2. EXPERIMENTAL DETAILS

2.1. Materials. All the chemicals were analytical grade and used as received without further purification. Titanium tetraisopropoxide (TTIP) [99.999%], tetrabutyl ammonium hydroxide (TBAH) [$(C_4H_9)_4NOH$ in 0.1 N aqueous], and mono/di/triethanolamine (MEA/DEA/TEA) were purchased from Merck.

2.2. Synthesis of TiO_2 NCs. TiO_2 NCs of different shapes were synthesized by varying the molar concentration ratio of TBAH to DEA using the hydrothermal method. In a typical synthesis of TiO_2 nanorods, 26.7 mL of TBAH and 10 mL of DEA (mol ratio 1:1) were taken in a 100 mL beaker and stirred for 10 min at 2−5 °C. Then 0.9 mL of TTIP (3 mmol) was added dropwise to this mixture of viscous liquid solution, stirred for another 3 min and brought to room temperature naturally. The white gummy viscous faintly precipitated solution was then transferred into a 50 mL Teflon-lined stainless steel autoclave and heated at 225 °C for 24 h. Then the autoclave was cooled down to room temperature under ambient conditions and the reaction mixture was centrifuged to collect the product. The as-synthesized product was washed successively with 0.1 N HCl, deionized water and ethanol several times to remove the organic molecules bound to the surface of the product. The final product was dried in air for 24 h at 60 °C. The other shapes of TiO_2 NCs were synthesized using the same methodology but by changing the molar ratio of TBAH to DEA.

2.3. Material Characterization. All the samples were calcined at 400 °C for 3 h in air before characterization and spectroscopic measurements. The surface morphology and microstructure of the products were examined by Carl Zeiss SUPRA or MERLIN field emission scanning electron microscope (FESEM) and TECNAI G2 (FEI) or JEM − 2100 (JEOL) transmission electron microscope (TEM) operated at 200 kV, respectively. The crystallographic phases of the as-synthesized products were obtained by a PANalytical high-resolution powder X-ray diffractometer (HR-XRD) [PW 3040/60] operated at 40 kV and 30 mA using Cu Kα X-rays. The Brunauer−Emmett−Teller (BET) surface area and UV−vis absorption measurements were carried out with ChemBET (Quantachrome Instruments) and Cary 5000 UV−vis-NIR spectrophotometer (Agilent Tech.), respectively. The Raman study was carried out with a SENTERRA dispersive Raman microscope (BRUKER). The X-ray photoelectron spectroscopy (XPS) was carried out by a Thermo-VG Scientific ESCALab 250 microprobe with a monochromatic Al Kα X-ray source (1486.6 eV).

2.4. Redox Activity Test. The redox photocatalytic property of the TiO_2 NCs was studied by a UV−vis absorption spectrophotometer (PerkinElmer Lamda 750). In a typical experiment, 20 mg of calcined catalyst (TiO_2 NCs) was dispersed in 45 mL of water and sonicated for 30 min. Then, 5 mL (5×10^{-5} M) of methyl orange (MO) or methylene blue (MB) was added to the suspended catalyst solution and sonicated for another 30 min in dark in order to saturate the adsorption−desorption of dye onto the catalyst surface. The resultant solution was irradiated under a low power 6 W ultraviolet (UV) light source for different durations at room temperature. The UV light source was placed 10 cm away from the catalyst mixed dye solution for all the experiments. The TiO_2 catalyst was separated by centrifuge prior to collecting the UV−vis absorption spectrum of irradiated dye solution.

3. RESULTS AND DISCUSSION

3.1. Surface Morphology. The surface morphology of TiO_2 NCs is found to significantly vary with the molar concentration ratio of bridging ligand (i.e., TBAH) to capping agent (i.e., DEA). Figure 1a−c shows the FESEM images of the as-synthesized TiO_2 nanorods, nanocapsules and nanocuboids, obtained at TBAH:DEA molar ratio of 1:1, 1:2, and 2:5, respectively, with all other synthesis parameters fixed (temperature 225 °C and hydrothermal reaction duration 24 h). Figure 1d shows the frequency of nanocuboids formed along with nanorods and nanocapsules at different concentration ratios of solvents. At an equal molar concentration of TBAH and DEA (TBAH:DEA = 1:1), growth of nanorods prevails over the nanocuboids as shown in Figure 1a. The length and width of these nanorods with elliptical ends are found to be 300−600 nm and 50−120 nm, respectively. On increasing the molar quantity of DEA (TBAH:DEA = 1:2), TiO_2 nanorods shrink along the axial direction to form nanocapsules as shown in Figure 1b, whereas there is a slight increase in the number density of nanocuboids. The length and width of TiO_2 nanocapsules are measured to be ∼200 nm and 80−100 nm, respectively. On further increasing DEA concentration (molar ratio TBAH:DEA = 2:5), only nanocuboids of size in range of 70−120 nm across diagonal are obtained, as shown in Figure 1c. The formation of rodlike TiO_2 NCs in the present study supports the previous report by Burnside et al. using similar chemicals and basic environment except DEA.[37] At higher

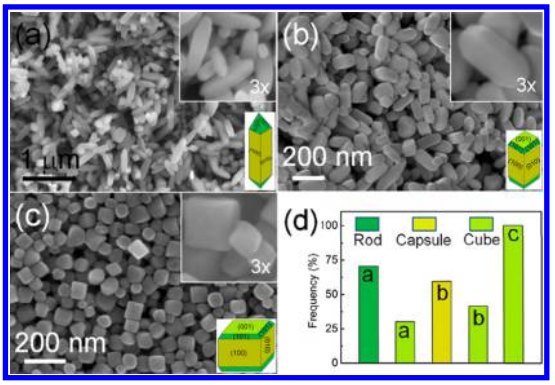

Figure 1. FESEM images of TiO_2 (a) nanorods, (b) nanocapsules, and (c) nanocuboids, obtained using the hydrothermal method with TBAH:DEA molar ratio of 1:1, 1:2, and 2:5, respectively. The other reaction parameters such as temperature (225 °C), duration (24 h) and TTIP precursor concentration (3 mmol) were kept constant. (d) Distribution graph for nanorods, nanocapsules, and nanocuboids obtained at different molar ratio of TBAH to DEA. The upper and lower insets of a−c show the corresponding magnified FESEM images and schematics, respectively, with different exposed facets of TiO_2 NCs.

synthesis temperatures (>230 °C) both the rodlike and bipyramidal morphology were reported whereas in the present work, DEA is used as shape-controlling agent to synthesize TiO_2 NCs of diverse morphologies. We have also varied the synthesis temperature in the range of 150−250 °C with molar ratio TBAH:DEA = 2:5 fixed. At a lower synthesis temperature of 150 °C, spherical particles of size <10 nm was obtained. The cuboid shape started to evolve at 200 °C and becomes prominent at 225 °C. However, at higher synthesize temperature (250 °C) particles are found to be bipyramidal shape. The effect of reaction duration on the formation of TiO_2 NCs is reported earlier.[34]

3.2. Microstructure and Exposed Facets Analysis. The microstructures, growth direction and different exposed facets of TiO_2 NCs were analyzed by TEM and high-resolution TEM (HRTEM). Figure 2a shows a TEM image of TiO_2 nanorods

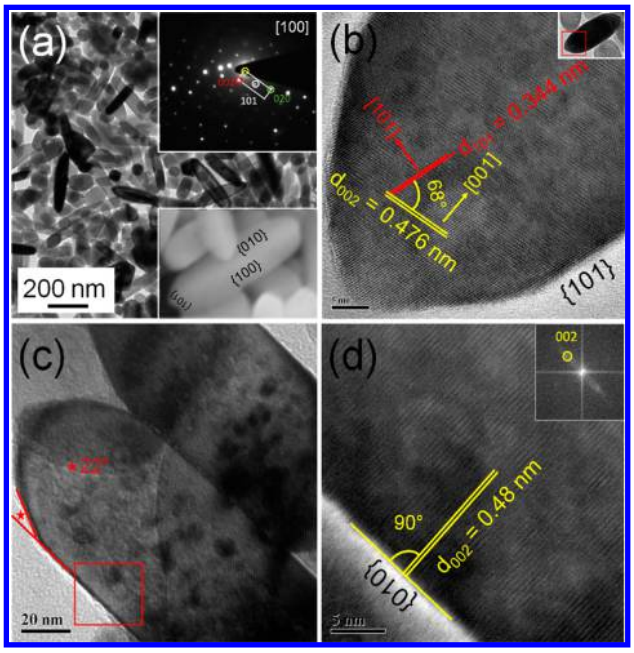

Figure 2. (a) TEM image of TiO_2 nanorods, (b) HRTEM image of the marked portion of a nanorod shown in the inset. (c) Magnified TEM image of nanorods with both the trunk and tip. (d) HRTEM image of the portion marked in (c). Upper inset of a shows the SAED pattern corresponding to b. Lower inset of a shows a representative magnified FESEM image with assigned facets. Inset of d shows the corresponding FFT pattern.

synthesized with TBAH:DEA = 1:1. The length and width of these rods vary in the range of 300−600 nm and 50−100 nm, respectively. Inset (upper) of Figure 2a shows the spots selected area electron diffraction (SAED) pattern indicating the single crystalline nature of the nanorods. The diffraction spots are indexed and matched the theoretical values with [100] zone axis.[38] As the surface free energy of anatase TiO_2 crystal follows the order $\gamma_{\{001\}} > \gamma_{\{100\}} > \gamma_{\{101\}}$, crystal growth normally occurs along [001] followed by [100].[39] The presence of (101) plane in the SAED pattern could be due to the NCs with (101) exposed planes. Figure 2(b) shows the HRTEM image taken on one end of a nanorod [shown in inset] indicating their exposed crystal planes. The lattice spacings at the pyramidal end of nanorod are measured to be 0.35 and 0.48 nm, which match the (101) and (002) planes of anatase TiO_2, respectively ([100] zone axis). This suggests that the sides of the pyramidal ends of nanorods are with {101} exposed facets, whereas there could be a very small portion of {001} exposed facets at the extreme pyramidal tip of nanorods. Figure 2c shows an angle (exterior) of 22° between trunk of a nanorod and its pyramidal head matching the theoretical angle 21.7° between (020) and (101) planes along [100] zone axis.[26] Figure 2d shows the HRTEM image of the portion marked in Figure 2c. The lattice spacing was found to be 0.48 nm corresponding to (002) planes and these planes are orthogonally aligned with the side edge of nanorod, suggesting {010} exposed facets at the middle portion of the rods (Figure 2d). Thus, the HRTEM analysis of the nanorods [Figure 2(b−d)] clearly suggests that the pyramidal tips are terminated with the thermodynamically stable {101} facets, whereas the trunk of the nanorods are with {010} exposed facets. The lower inset of Figure 2a represents an FESEM image of the nanorods assigned with different exposed facets.

Figure 3a shows a TEM image of capsule shape TiO_2 NCs obtained with TBAH:DEA = 1:2. The length and width of

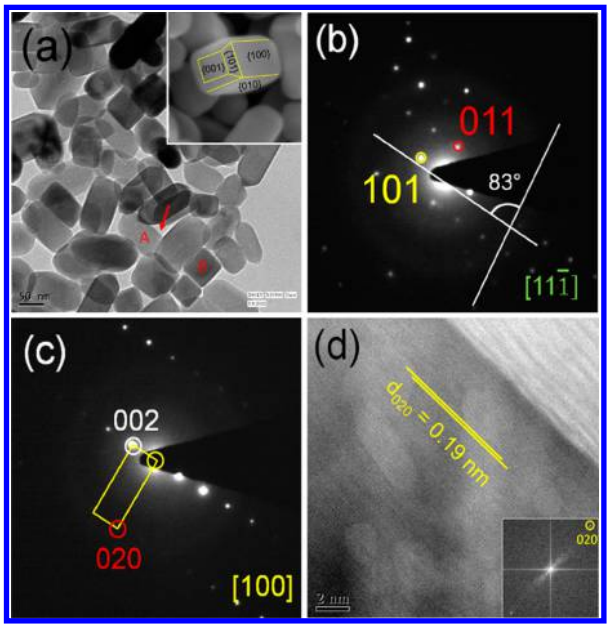

Figure 3. (a) TEM image of TiO_2 nanocapsules. (b, c) SAED patterns taken in the region B and A in image a, respectively. (d) HRTEM image of a nanocapsule taken from the region marked by the arrow in image a. Inset of a shows a representative FESEM image with exposed crystal facets and inset of d shows the corresponding FFT pattern.

these capsule shape TiO_2 NCs vary in the range of 200−300 nm and 80−150 nm, respectively. The decrease in length and increase in width of the capsules as compared to the rods indicate increase (decrease) in growth along [100] ([001]). Figure 3(b) shows the SAED spots pattern along [11$\bar{1}$] zone axis taken from the region marked as B in Figure 3a. The SAED pattern indicates the single crystalline nature and assigned diffraction spots match the theoretical values.[40] Figure 3c shows a SAED pattern along [100] of the region marked as A in Figure 3a. Figure 3d shows the HRTEM image of a TiO_2 nanocapsule taken from the region marked by an arrow in Figure 3a which is projected along [100] [as per SAED analysis, Figure 3c]. The distance between two consecutive planes at the edge of a capsule is measured to be 0.19 nm (also parallel to nanocapsule body), corresponding to the distance between (020) planes of anatase TiO_2 ([100] zone axis). This suggests

that the top/bottom end and sides of the capsules are high-energy {001} and {100}/{010} exposed facets, respectively. A representative FESEM image of capsule with assigned facets is shown as inset of Figure 3a.

Figure 4a shows a TEM image of nanocuboids obtained with TBAH:DEA = 2:5, keeping other experimental parameters

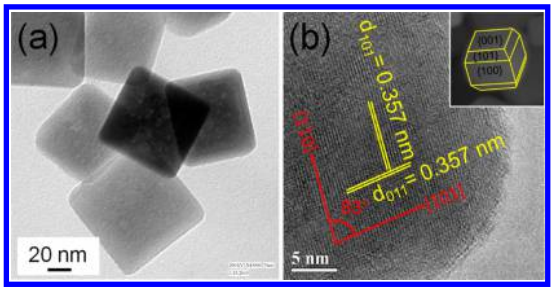

Figure 4. (a) TEM image of TiO_2 nanocuboids obtained at TBAH:DEA = 2:5 (reaction temperature and duration were 225 °C and 24 h, respectively). (b) HRTEM image of a nanocuboid with the measured lattice spacing and angle between the planes. Inset shows an FESEM image with assigned crystal planes.

fixed. The size of these nanocuboids varies in the range of 70−130 nm along diagonal. The FESEM and TEM analysis clearly reveal that with increasing the TBAH:DEA ratio from 1:2 (capsule shape TiO_2 NCs) to 2:5, the NCs growth further decreases along [001] and increases slightly along [100] producing cuboid shape TiO_2 NCs. The lattice fringe from a nanocuboid is shown in Figure 4b. The lattice spacings of 0.357 nm are lying with an angle of 83°, matching the spacing between (101) and (011) planes with $[11\bar{1}]$ zone axis, which confirms the top and bottom of the cuboids with {001} exposed facets.[40] A representative FESEM image (inset of Figure 4b) shows different exposed facets of a cuboid shape TiO_2 NC correlating with the HRTEM analysis.

The detail FESEM and HRTEM analysis above showed that with increase in DEA molar quantity, morphology of NCs evolves from rods to cuboids and the growth of NCs decreases along [001]. For further clarity and to ensure the exact role of DEA on the growth direction as well as exposed facets of TiO_2 NCs, we synthesized TiO_2 NCs using very low (TBAH:DEA = 10:1) and very high quantity (TBAH:DEA = 1:10) of DEA. Figure 5a shows the ellipsoid shape TiO_2 NCs obtained with low DEA quantity (TBAH:DEA=10:1) keeping other reaction parameters fixed (TTIP precursor 3 mmol, temperature 225 °C, reaction duration 24 h). Inset of Figure 5a shows the SAED spots pattern of the TiO_2 NCs which are assigned and matched the (101), (001), and (220) planes.[20] At this very low DEA and high TBAH molar quantity, NCs growth takes place mainly along high-energy [110] and [001] as they are thermodynamically favored growth direction of anatase TiO_2 compared to low-energy [101]. Figure 5b shows a HRTEM image with measured lattice spacing of 0.35 nm corresponding to (101) planes. This indicates that nanoellipsoids are enfolded with low energy {101} facets producing the thermodynamic stable NCs under almost unrestricted crystal growth. Similarly, TiO_2 NCs synthesized with a very high DEA quantity (TBAH:DEA = 1:10) are of sheet-type and particle-like morphology as shown in Figure 5(c). The size of nanosheets varies in the range of 30−60 nm across diagonal and is found to be the smallest among all the NCs. Inset of Figure 5c shows the SAED pattern of TiO_2 nanosheets along $[11\bar{1}]$ zone axis.[40] The careful

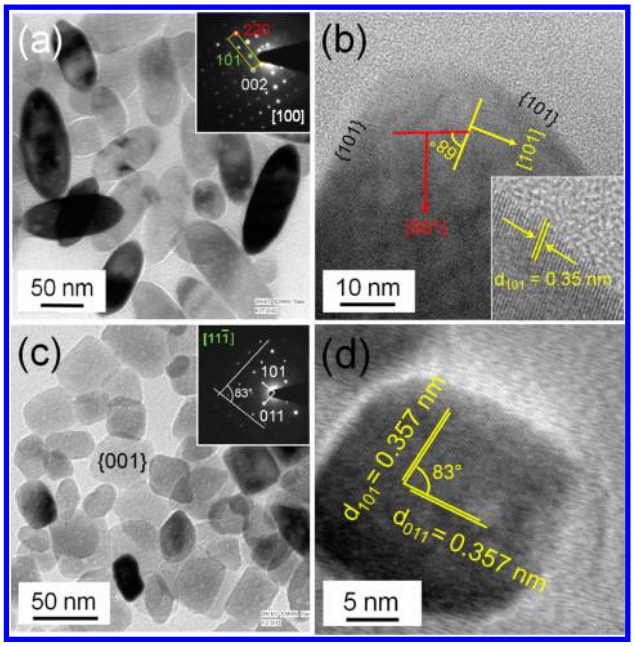

Figure 5. TEM and HRTEM images of (a, b) ellipsoid shape, and (c, d) sheetlike TiO_2 NCs obtained at TBAH:DEA = 10:1 and 1:10, respectively. Insest of a and c show the corresponding SAED pattern. Inset of b shows magnified HRTEM image with the lattice fringe.

observation of the SAED pattern reveals the crystal growth along the unfavorable [101] direction which exposes high-energy {001} facets to an extreme extent further supported with Raman spectroscopy (discussed later).[39] The HRTEM analysis also suggests the same interpretation (Figure 5d).[40,41] The lattice spacing are lying with an angle 83° and the spacings are found to be 0.357 and 0.357 nm, respectively corresponding to (101) and (011) planes of anatase TiO_2 crystal.[40,41] This suggests that the top and bottom of the sheetlike particles with {001} exposed facets. Thus, at very low and high concentration of DEA, TiO_2 NCs with maximum low-energy {101} and high-energy {001} exposed facets are obtained by restricting the crystal growth along the same planes, respectively.

The different facets of TiO_2 NCs are known to have different chemical environments which prompted the researchers to control its exposed facets.[22,25] The {001} and {101} exposed facets of TiO_2 NCs are made up of 100% and 50% Ti_{5c}, respectively.[22,25] Thus, TiO_2 NCs with larger {001} exposed facets area have higher bending vibration whereas TiO_2 NCs with {101} exposed facets have higher stretching vibration. Such facets sensitive behavior has been obtained using the intensity of different Raman scattering from TiO_2 NCs.[42] The HRTEM and FESEM analysis revealed that the surface area of {001} facets increases with increase in the DEA quantity keeping other reaction parameters fixed. The exposed nature of {001} facets for TiO_2 NCs was further ascertained by the Raman spectroscopy. Figure 6 shows the Raman spectra of TiO_2 NCs with diverse shapes. The frequencies of five major Raman bands observed at 142, 196, 395, 514, and 637 cm^{-1} are assigned as $E_g(1)$, $E_g(2)$, $B_{1g}(1)$, $B_{1g}(2)+A_{1g}$, and $E_g(3)$ vibration modes, respectively.[43,44] The B_{1g} to E_g intensity ratio is found to be increased by a factor of more than 300% with the change in TiO_2 NCs shape from nanoellipsoids to nanosheets (Table 1). This increment is attributed to increase of the bending vibration from nanoellipsoids to nanosheets,

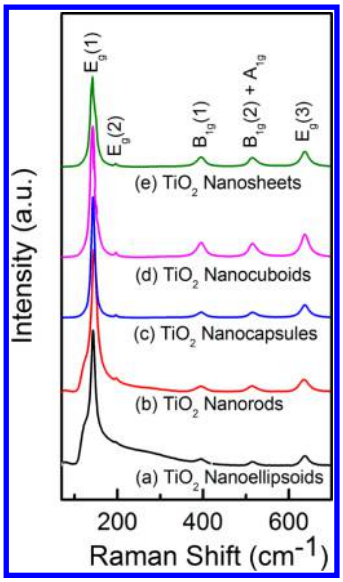

Figure 6. Raman spectra of TiO_2 (a) nanoellipsoids, (b) nanorods, (c) nanocapsules, (d) nanocuboids, and (e) nanosheets obtained with TBAH:DEA molar ratio of 10:1, 1:1, 1:2, 2:5, and 1:10 respectively, using the hydrothermal method at 225 °C in 24 h.

Table 1. Intensity Ratio of Symmetric Bending (B_{1g}) to Symmetric Stretching (E_g) Vibration Raman Modes of TiO_2 NCs with Different Exposed Facets

morphology	$[B_{1g}/E_g]_{\text{symmetric vibration}}$	% increment
nanoellipsoids	0.027	0
nanorods	0.038	40.7
nanocapsules	0.045	66.6
nanocuboids	0.113	318.5
nanosheets	0.126	366.6

which is due to the increase in the surface area of high-energy {001} exposed facets.[42]

The Raman analysis on TiO_2 NCs with different exposed facets is further compared with the XRD analysis. Figure 7 shows the XRD patterns of different TiO_2 NCs. The XRD patterns of TiO_2 NCs with different morphologies are matched the reference pattern (JCPDS 00−002−0387) of pure

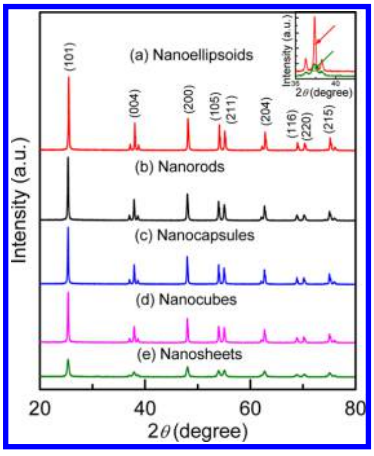

Figure 7. XRD patterns of (a) nanoellipsoids, (b) nanorods, (c) nanocapsules, (d) nanocuboids, and (e) nanosheets obtained with TBAH:DEA molar ratio of 10:1, 1:1, 1:2, 2:5, and 1:10 respectively, using the hydrothermal method at 225 °C in 24 h.

crystalline tetragonal anatase TiO_2. However, the intensity ratios of different diffraction features are found to vary with the morphology of the TiO_2 NCs. In particular, the relative XRD intensity ratio i.e., $I_{(004)}/I_{(200)}$, is found to be maximum for nanorods (obtained with low DEA quantity) and minimum for nanosheets (obtained with high DEA quantity), indicating strong and weak growth along [001] (along the *c*-axis), respectively (Table 2).[45,46] The symbol $I_{(004)}$ and $I_{(200)}$ denote

Table 2. Comparison of XRD Intensities from Different Planes of TiO_2 NCs with Different Morphology

morphology	$I_{(004)}/I_{(200)}$
nanoellipsoids	0.74
nanorods	0.80
nanocapsules	0.79
nanocuboids	0.64
nanosheets	0.46

the XRD intensity of (004) Bragg peak at 38.0° and of (200) peak at 48.1°, respectively. Furthermore, full width at half-maximum of the diffraction peaks from nanosheets is found to be at least 4 times broader than that of ellipsoids as shown in the inset of Figure 7. This broadening of diffraction feature for TiO_2 nanosheets is due to the least growth along [001] and smaller size.

3.3. Growth Mechanism of TiO_2 NCs. The formation of TiO_2 NCs from the alkoxide precursors takes place in two important steps: (a) hydrolysis of titanium precursor to form hydroxyalkoxide and (b) their subsequent condensation to form Ti−O−Ti skeleton. The bridging ligand and capping agent play prime role in the above-mentioned steps to control the shape and size of NCs. Bridging ligand supplies water molecules or hydroxyl groups, and its concentration determines the hydrolysis rate. A capping agent is used to prevent Ti−O−Ti skeletal growth three dimensionally. As per the FESEM, HRTEM, Raman, and XRD analysis, the growth of different shapes of TiO_2 NCs has been demonstrated. At the center of Figure 8, a unit cell of anatase TiO_2 is illustrated. Among the facets of TiO_2 crystal, as {110}, {001}, and {100} facets contain higher surface energy than that of {101} facets, growth usually occurs along those facets exposing {101} facets under an unrestricted condition. In order to grow TiO_2 crystals with high-energy exposed facets, it is necessary to provide restriction to the growth along the same facets, i.e., {110}, {001}, and {100}. One of the possible ways to achieve the desired goal is capping of the high-energy facets selectively during the crystal growth. Such capping of the high-energy facets compels the crystals to grow along unfavorable low-energy facet, i.e., {101}, thereby forming crystals with high-energy exposed facets. The morphology change in the order of nanoellipsoids → nanorods → nanocapsules → nanocuboids → nanosheets is attributed to selective binding of DEA onto the high-energy {001} facets. With a lower molar concentration of DEA (i.e., TBAH:DEA = 10:1), growth and hydrolysis predominates along the high-energy facets [110] and [001] over capping forming nanoellipsoids (Figure 5a, b) with maximum {101} exposed facets. With 1:1 TBAH:DEA molar ratio, DEA could cap a smaller percentage of {001} facets, thereby producing ∼30% of nanocuboids (Figure 1a, d). However, the remaining TiO_2 NCs grew along [001], leading to ∼70% of nanorods with major {100}/{010} exposed facets (Figures 1a and 2). With increasing DEA (i.e., TBAH:DEA = 1:2), capping on {001}

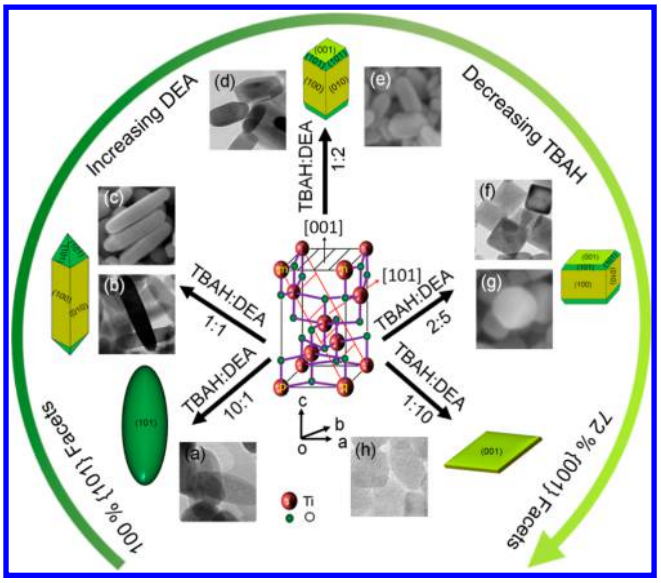

Figure 8. Schematics of anatase TiO_2 unit cell evolving to diverse shape of TiO_2 NCs by varying the molar concentration ratio of TBAH to DEA. The (001), and (101) planes of the unit cell are shown by parallel black, and red lines, respectively. For clarity and simplicity, (100) plane is designated by upward m,n,p,q Ti atoms. Representative (a, b, d, f, h) TEM and (c, e, g) FESEM images of (a) nanoellipsoids, (b, c) nanorods, (d, e) nanocapsules, (f, g) nanocuboids, and (h) nanosheets.

facets increases and the crystal growth slightly decreases along the same direction. However, the crystal growth slightly increases along [100] (as the surface energy of {100} facets is next to the {001} facets of anatase TiO_2), exposing the high-energy {001} facets to some extent and producing capsule shape TiO_2 NCs with major {100} and minor {001} exposed facets (Figures 1b and 3). In addition, the percentage of nanocuboids increases to 40% (Figure 1d) as expected. On further increasing the molar quantity of DEA (TBAH:DEA = 2:5), capping increases on the high-energy {001} facets and crystal growth occurs along all the major facets (i.e., {001}, {100}, and {101}), producing 100% nanocuboids (Figures 1c and 4) with all these exposed facets. However, with a much higher DEA molar concentrations (TBAH:DEA = 1:10), TiO_2 nanosheets with the primary growth along [101] are obtained (Figure 5c, d). This is due to the strong DEA capping on {001} facets with complete suppression of growth along that direction forming sheet-like morphology (with maximum high-energy {001} exposed facets). In Figure 8, we summarize the growth evolution of TiO_2 NCs by varying the bridging ligand (TBAH) to capping agent (DEA) ratios. The percentage of exposed facets surface area of TiO_2 NCs with different morphologies is calculated as per the reported procedure (see the Supporting Information) and presented in Table 3.[26]

3.4. Role of Amines. The amine compounds are known to have intense affinity toward TiO_2 surfaces and thus used as capping agent.[30,47] The capping of amines is ascribed to the presence of 2-fold coordinated oxygen (2c-O) and 100% 5-fold coordinated titanium (5c-Ti) atoms on the {001} TiO_2 facet, making it much more reactive than that of {101} facet, which has 50% 5c-Ti atoms. Therefore, strong H-bonding could occur between the polar-Hs of amine with two consecutive 2c-O atoms on the {001} TiO_2 facet stabilizing it. We have used three different amines (MEA, DEA, and TEA) to find their effective role as capping agent. The different amine structures were optimized by the density functional theory (DFT) calculation (see Figure S1 in the Supporting Information). From the DFT calculation, the distances between polar-Hs (OH and NH) of the optimized DEA structure are found to be 0.46 and 0.44 nm (see Figure S1 in the Supporting Information). Theoretical study showed that in a relaxed state, the distance between two consecutive 2c-O atoms of {001} TiO_2 facet is 0.53 nm, that of {101} facet is 0.28 nm.[24,26,48] As the distances between polar-Hs of DEA are close to the distances between two consecutive 2c-O atoms of {001} facet (0.53 nm) than that of two consecutive 2c-O of {101} facet (0.28 nm), it is obvious that DEA could interact exclusively with 2c-O atoms of {001} TiO_2 facet through H-bonding and not interact with the 2c-O atoms of other facets as their interatomic distances are not well-matched. To verify the above arguments, we show the TiO_2 NCs obtained with either MEA or TEA as capping agents. It was found that MEA and TEA cap the high-energy facets very poorly resulting in the ellipsoids (see Figure S2a, b in the Supporting Information) and ellipsoids with very few cuboids TiO_2 NCs (see Figure S2c, d in the Supporting Information), respectively, at molar ratio of TBAH:MEA/TEA = 2:5, keeping other reaction parameters fixed. The negligible and partial capping by MEA and TEA, respectively, can be attributed to the distances between polar-H atoms in the respective molecules with the distance between 2c-O atoms on the {001} TiO_2 facet. From Figure S1 in the Supporting Information, it is observed that TEA is larger in size than that of MEA/DEA, and the distance between one pair of polar-Hs of TEA (0.51 nm) is closely match the distance between the two consecutive 2c-O atoms of {001} TiO_2 facet (0.53 nm), which is believed to be involved in partially capping and thereby producing a few nanocuboids (see Figure S2c, d in the Supporting Information). However, the distance between polar-H atoms of MEA (0.24 and 0.25 nm) are rather matched the distance between the two consecutive 2c-O atoms of {101} TiO_2 facet (i.e., 0.28 nm). Therefore, MEA could cap {101} facets forming elongated shape crystals unlike the DEA, which caps the {001} facets to form nanocuboids and nanosheets with

Table 3. Comparison of Photoredox Activity with BET Surface Area (Physical Property), Bandgap (Electronic Property), and Exposed Facets (Chemical Property) of TiO_2 NCs

morphology	BET surface area (m^2/g)	bandgap (eV)	% of {101} facets	% of {001} facets	% of {100} facets	k_{MO} (h^{-1} S^{-1})	k_{MB} (h^{-1} S^{-1})
nanoellipsoids	11.25	3.16	~100	0	0	0.048	0.070
nanorods	6.22	3.17	25	0	75	0.220	0.150
nanocapsules	18.92	3.07	13	14	73	0.073	0.060
nanocuboids	22.05	3.21	25	28	47	0.078	0.099
nanosheets	60.23	3.05	0	72	28	0.015	0.019
Degussa P25	51.58					0.059	0.048

{001} exposed facets strongly supporting the experimental results. The present results suggest DEA as a major morphology control agent in producing TiO_2 NCs. However, other experimental parameters such as temperature and duration could have a slight effect on the same.

3.5. Photocatalytic Redox Activity. The photocatalytic activity of TiO_2 NCs is demonstrated by the degradation of MO and MB dyes in the presence of UV light. Before UV light irradiation, the catalyst-dye solutions were kept in dark for 30 min to reach the dye's adsorption−desorption equilibrium on the catalyst surface. The dye degradation takes place in two steps: (i) first adsorption of dye molecules on the TiO_2 surface and (ii) e^-/h^+ transfer to the TiO_2 surface to cleave the hazardous molecules upon light irradiation. Higher the surface area, higher will be the adsorption of dye and probability of degradation. Therefore, it is necessary to compare the degradation performance with the surface area of TiO_2 to get an idea about the exact surface specific activity of a catalyst.[21,49] The photocatalytic activity was measured using UV−vis absorption spectroscopy. Figure S3 and S4 (see the Supporting Information) show the UV−vis absorption plots of MO and MB, respectively, as a function of irradiation time in the presence of different TiO_2 NCs. Figure 9a shows the rate

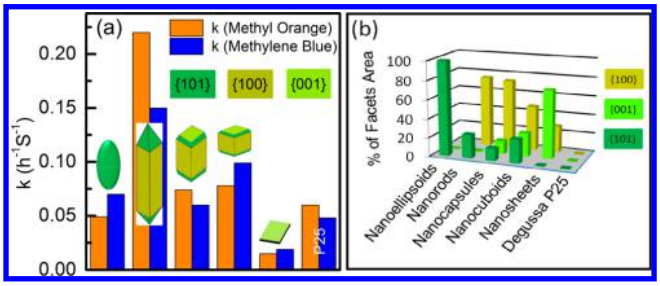

Figure 9. (a) Photocatalytic activity of TiO_2 NCs with different shapes for the degradation of MO and MB. The rate constants values are compared with the specific surface area as dye degradation follows the adsorption onto the catalyst surface prior to degradation in the presence of light. (b) Relative % of exposed facets area of TiO_2 NCs with different shapes.

constants of MO and MB degradation estimated from the linearly fitted curve of $\ln(C_0/C)$ vs irradiation time, where "C_0" and "C" are the dye concentration before and after irradiation, respectively. The photocatalytic activity (rate constant) of the nanorods enclosed with ~25% {101} facets and ~75% {100}/{010} facets (Figure 9b) was found to be 3.7 and 14.6 times higher than that of the commercial Degussa P25 and nanosheets, respectively, for the degradation of MO per specific surface area of TiO_2 NCs. Similarly, nanorods exhibit 3.1 and 7.8 times higher activity than the Degussa P25 and nanosheets for the degradation of MB, respectively.

The photodegradation of dyes by TiO_2 has been studied enormously due to its unique surface mediated green protocol. But the details of this mineralization or the exact role of photogenerated carriers (e^-/h^+) and/or the major factor that determines the rate of degradation processes are still ambiguous.[50−52] The degradation nature of these small hazardous molecules follows complex manner with different intermediates.[50,51] The previous study showed that degradation of MO (see Figure S5a in the Supporting Information) takes place through an important hydroxylated intermediate as shown in Figure S5b in the Supporting Information.[53] This hydroxylated intermediate is nothing but the substitution in a benzene ring of MO, which is formed by the attack of hydroxyl radical generated on TiO_2 NC's surface. Similarly, the degradation of MB (see Figure S5c in the Supporting Information) is believed to be followed by the important ring opening intermediate (see Figure S5d in the Supporting Information) that is formed upon reduction of MB to amine functional derivative. The photodegradation of MO and MB on TiO_2 NC's surface are photooxidative and photoreductive cleavage, respectively.[52−56] Thus, the pick point ought to be the intermediate formation step of degradation and thus the rate-determining step. The important steps of oxidative hydroxyl radical and reductive superoxide ion formation on TiO_2 surface in the presence of photogenerated carriers and the subsequent formation of dye intermediates is as follows

$$TiO_2 + h\nu \rightarrow TiO_2(e^- + h^+) \quad (1)$$

$$H_2O + h^+ \rightarrow OH^\bullet + H^+ \quad (2)$$

$$O_2 + e^- \rightarrow O_2^- \quad (3)$$

$$MO + OH^\bullet \rightarrow \text{hydroxylated} - MO + H^\bullet \quad (4)$$

$$MB + 3H^+ + O_2^- + 3e^- \rightarrow \text{reductive amine} \quad (5)$$

Recently, different strategies have been taken into consideration to improve the photocatalytic activity of TiO_2, e.g., preparing porous and/or mesopoprous TiO_2 NCs or doping with suitable metals or nonmetals or increasing the surface area of high-energy {001} or {100} exposed facets.[22,57−59] But the fundamental role of photogenerated carriers and facets-dependent redox activity of TiO_2 NCs are not studied in detail. In the present work, the redox activity of TiO_2 NCs is correlated with physical (BET surface area), electronic (valence band position and bandgap) and chemical (exposed facets) properties, and compared with the photocatalytic activity per unit surface area due to the heterogeneous nature of the degradation kinetics. The enhanced photocatalytic activity of the porous or mesoporous TiO_2 NCs is attributed to their high BET surface area, i.e., related to the physical property that does not increase its intrinsic photocatalytic activity.[58,60] The doping and coating of TiO_2 with metals or nonmetals change the chemical composition as well the electronic properties, i.e., those are related to the chemical and electronic properties, but not related with the increase of photoredox activity of pristine TiO_2.[61] On the other hand, chemical environment of different facets of TiO_2 NCs has in turns significant effects on the electronic property of pristine TiO_2.[22,25] As the electronic band position, BET surface area and exposed facets are related to the photocatalytic activity, we carefully considered all these factors to evaluate the role of surface chemistry onto the intrinsic photocatalytic activity of TiO_2 NCs. The BET surface area (Table 3) was found to be in the order of nanosheets ≫ nanocuboids ~ nanocapsules ~ nanoellipsoids > nanorods. The optical and electronic properties of NCs were measured from the UV−vis absorption spectra (see Figure S6 in the Supporting Information) and valence band (VB) XPS spectra (Figure 10), respectively. The UV−vis measurement indicates that the TiO_2 nanosheets have slightly lower bandgap than that of NCs with other morphology. As the VB maxima position of all the NCs were almost at same binding energy of 2.3 eV, the CB minima was accordingly placed as shown in Figure 11. Although, this upward shift of CB edge (in electrochemical

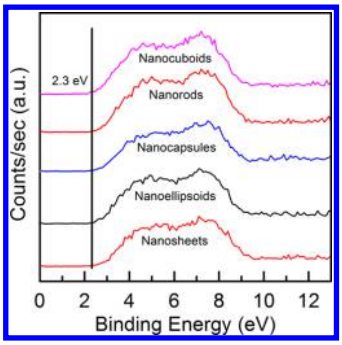

Figure 10. VB XPS spectra of TiO_2 NCs with different shapes. The VB position is found to be almost the same regardless of shapes and exposed natures of the TiO_2 NCs.

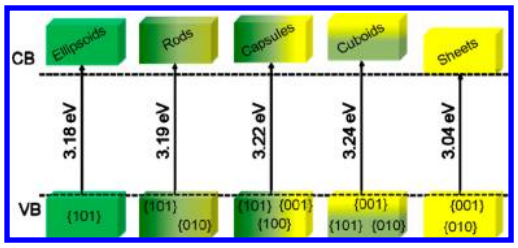

Figure 11. Schematic of electronic band positions of different shape TiO_2 NCs with different exposed facets as marked in their respective valence bands.

scale) for NCs with (001) exposed facets supports the previous XPS results by Pan et al.,[25] it contradicts the negative shift of flatband potential.[62] The phototocatalytic properties of TiO_2 NCs with different exposed facets also strongly depend on its flatband potential. In particular, the spectroelectrochemical studies confirmed a negative shift of flatband potential for the TiO_2 NCs with (001) exposed facets leading to a larger open-circuit potential of the solar cell. The negative shift of flatband potential can also be corroborated to improved Li insertion on (001)-oriented nanosheets.[63] Therefore, extensive studies needed in order to gain further insights on the VB and CB positions of TiO_2 NCs. The width of VB feature (Figure 10) is measured to be nearly same, i.e., 6.7 eV for the TiO_2 NCs with diverse shapes, suggesting similar mobilities of charge carriers.[25] On the basis of VB position (electronic property), the photoredox activity of the TiO_2 nanosheets ought to be the highest among all. Interestingly, experimental finding revealed that the photoredox activity of TiO_2 nanorods is >3 times than that of TiO_2 nanosheets and commercial catalyst Degussa P25.

A comparative study on the physical, chemical, and electronic properties of different TiO_2 NCs is shown in Table 3. The BET surface area is highest for nanosheets (60.23 m^2/g) whereas lowest for nanorods (6.22 m^2/g). On the other hand, UV–visible (see Figure S6 in the Supporting Information) and VB electronic structure (Figure 10) show that the bandgap of nanosheets is least whereas it is highest for nanocuboids. The highest photocatalytic activity of TiO_2 nanorods is believed to be the unique surface chemistry of {100}/{010} facets, which could have synergistic effects with the {101} facets as the nanorods are enclosed by {101} and {100}/{010} facets.[25,34] Moreover, TiO_2 NCs exposed with low-energy {101} facets only (ellipsoid shape TiO_2 NCs) or high-energy {001} facets only (sheet-like TiO_2 NCs) exhibit poor photocatalytic activity. Recently, it was reported that TiO_2 NCs with only high-energy {001} or {100}/{010} exposed facets show poor photocatalytic activity than the TiO_2 NCs with both high-energy {001}, {100}/{010} and low-energy {101} exposed facets.[34,64] The reason for synergistic effects of the different facets of TiO_2 NCs could be due to the difference in surface chemistry of the different facets. The presence of 100% 5c-Ti and 2c-O atoms on high-energy {100}/{010} and {001} facets makes them craving for positively charged h^+. On the other hand, low-energy {101} facets are known to be accumulated with negatively charged e^- when excited under UV-light.[35,36] Because of such a synergy effect, we showed in our previous report that the presence of low-energy {101} facets is evenly important along with the high-energy {001}/{100} facets for improved photocatalysis.[34] Thenceforth many theoretical as well experimental works have been acceding the notion of the carrier separation through synergy effects of crystal facets.[64−67] In particular, Ma et al. and Nunzi et al. showed that the large difference in trapping energy of the carriers on different facets could allow the low recombination and hence higher quantum yield.[65,67] But it was difficult to clarify whether {001} or {100} facets plays a crucial role for separating the excited carriers more efficiently. In this study, the intrinsic photoredox activity of rod shape TiO_2 NCs is found to be 2.8 and 1.5 times higher than the cuboid shape TiO_2 NCs with {001} and {101} exposed facets. The higher activity of rod shape TiO_2 NCs is therefore believed to be due to the higher synergistic effects of {100}+{101} facets than that of the {100}+{001}+{101} facets. On the other hand, capsule shape TiO_2 NCs shows poor activity although made up of majorly {100}/{010} facets. The lower intrinsic activity of capsule shape attributes the lack of enough reductive {101} facets which is essential for the carrier separation. Thus, the intrinsic photocatalytic activity of different facets of TiO_2 NCs can be ranked as {101}+{100}/{010} > {101}+{001}+{100}/{010} > {101} > {001}.

4. CONCLUSIONS

In summary, DEA is demonstrated as a powerful shape-controlling reagent in place of environmentally unfriendly HF to selectively cap the high-energy {001} facets of TiO_2 NCs. With increasing the DEA concentration in the reaction medium, growth along the [001] is arrested and morphology follows the order nanoellipsoids → nanorods → nanocapsules →nanocuboids → nanosheets. The detailed growth of NCs, their characterization, and photoredox activity were tested. In spite of smaller bandgap of TiO_2 nanosheets along with high-energy {001} exposed facets, the highest photocatalytic activity was obtained from nanorods. The nanorods exhibit 3.7 times higher photo-oxidation of MO and 3.1 times greater photo-reduction of MB than that of the commercial photocatalyst Degussa P25. The enhanced photoredox activity from nanorods is ascribed to the unique surface chemistry of {100}/{010} facets which enhances the efficient charge separation in the presence of low-energy reductive {101} exposed facets. The intrinsic photocatalytic activity of different facets of TiO_2 NCs are found to be in the order of {101}+{100}/{010} > {101}+{001}+{100}/{010} > {101} > {001}, which is well-correlated with the theoretical predictions of TiO_2 NC facets.

■ ASSOCIATED CONTENT

Supporting Information

Optimized structure of amines using Gaussview 5.0.9. TEM images. UV–vis absorption spectra of MO and MB irradiated solutions. Structure of MO and MB, and their oxidative/reductive intermediates. UV–vis absorption spectra of TiO_2

NCs. Relative surface area estimation of TiO_2 NCs exposed facets. This material is available free of charge via the Internet at http://pubs.acs.org.

AUTHOR INFORMATION

Corresponding Author

*E-mail: deb@matsc.iitkgp.ernet.in.

Notes

The authors declare no competing financial interest.

ACKNOWLEDGMENTS

This work was funded by the Department of Science and Technology, New Delhi, India (Indo Korea/P-02) and National Research Foundation of Korea, MEST (2012-0006296). N.R. acknowledges CSIR, New Delhi for the financial support through CSIR scholarship. K.T.L. is grateful for the support of the Natural Sciences and Engineering Research Council of Canada.

REFERENCES

(1) Wang, X. H.; Li, J.-G.; Kamiyana, H.; Moriyoshi, Y.; Ishigaki, T. Wavelength-Sensitive Photocatalytic Degradation of Methyl Orange in Aqueous Suspension over Iron(III)-doped TiO_2 Nanopowders under UV and Visible Light Irradiation. *J. Phys. Chem. B* **2006**, *110*, 6804−6809.

(2) Pearson, A.; Jani, H.; Kalantar-zadeh, K.; Bhargava, S. K.; Bansal, V. Gold Nanoparticle-Decorated Keggin Ions/TiO_2 Photocatalyst for Improved Solar Light Photocatalysis. *Langmuir* **2011**, *27*, 6661−6667.

(3) Lee, W. J.; Lee, J. M.; Kochuveedu, S. T.; Han, T. H.; Jeong, H. Y.; Park, M.; Yun, J. M.; Kwon, J.; No, K.; Kim, D. H.; Kim, S. O. Biomineralized N-Doped CNT/TiO_2 Core/Shell Nanowires for Visible Light Photocatalysis. *ACS Nano* **2012**, *6*, 935−943.

(4) Li, H.; Cheng, J.-W.; Shu, S.; Zhang, J.; Zheng, L.; Tsang, C. K.; Cheng, H.; Liang, F.; Lee, S.-T.; Li, Y. Y. Selective Removal of the Outer Shells of Anodic TiO_2 Nanotubes. *Small* **2013**, *9*, 37−44.

(5) Duan, Y.; Fu, N.; Liu, Q.; Fang, Y.; Zhou, X.; Zhang, J.; Lin, Y. Sn-Doped TiO_2 Photoanode for Dye-Sensitized Solar Cells. *J. Phys. Chem. C* **2012**, *116*, 8888−8893.

(6) Kim, Y.-G.; Walker, J.; Samuelson, L. A.; Kumar, J. Efficient Light Harvesting Polymers for Nanocrystalline TiO_2 Photovoltaic Cells. *Nano Lett.* **2003**, *3*, 523−525.

(7) Grzmil, B.; Glen, M.; Kic, B.; Lubkowski, K. Preparation and Characterization of Single-Modified TiO_2 for Pigmentary Applications. *Ind. Eng. Chem. Res.* **2011**, *50*, 6535−6542.

(8) Wang, Y.; Li, J.; Wang, L.; Xue, T.; Qi, T. Preparation of Rutile Titanium Dioxide White Pigment via Doping and Calcination of Metatitanic Acid Obtained by the NaOH Molten Salt Method. *Ind. Eng. Chem. Res.* **2010**, *49*, 7693−7696.

(9) Hensel, J.; Wang, G.; Li, Y.; Zhang, J. Z. Synergistic Effect of CdSe Quantum Dot Sensitization and Nitrogen Doping of TiO_2 Nanostructures for Photoelectrochemical Solar Hydrogen Generation. *Nano Lett.* **2010**, *10*, 478−483.

(10) Sayed, F. N.; Jayakumar, O. D.; Sasikala, R.; Kadam, R. M.; Bharadwaj, S. R.; Kienle, L.; Schürmann, U.; Kaps, S.; Adelung, R.; Mittal, J. P.; Tyagi, A. K. Photochemical Hydrogen Generation Using Nitrogen-Doped TiO_2−Pd Nanoparticles: Facile Synthesis and Effect of Ti^{3+} Incorporation. *J. Phys. Chem. C* **2012**, *116*, 12462−12467.

(11) Park, J.; Yi, J.; Tachikawa, T.; Majima, T.; Choi, W. Guanidinium-Enhanced Production of Hydrogen on Nafion-Coated Dye/TiO_2 under Visible Light. *J. Phys. Chem. Lett.* **2010**, *1*, 1351−1355.

(12) Kobayashi, M.; Petrykin, V. V.; Kakihana, M. One-Step Synthesis of TiO_2(B) Nanoparticles from a Water-Soluble Titanium Complex. *Chem. Mater.* **2007**, *19*, 5373−5376.

(13) Qu, Q.; Geng, H.; Peng, R.; Cui, Q.; Gu, X.; Li, F.; Wang, M. Chemically Binding Carboxylic Acids onto TiO_2 Nanoparticles with Adjustable Coverage by Solvothermal Strategy. *Langmuir* **2010**, *26*, 9539−9546.

(14) Nian, J.; Teng, H. Hydrothermal Synthesis of Single-Crystalline Anatase TiO_2 Nanorods with Nanotubes as the Precursor. *J. Phys. Chem. B* **2006**, *110*, 4193−4198.

(15) Stathatos, E.; Lianos, P.; Monte, F. D.; Levy, D.; Tsiourvas, D. Formation of TiO_2 Nanoparticles in Reverse Micelles and Their Deposition as Thin Films on Glass Substrates. *Langmuir* **1997**, *13*, 4295−4300.

(16) Yu, C. Y.; Zhang, L.; Yu, J. Rapid Synthesis of Mesoporous TiO_2 with High Photocatalytic Activity by Ultrasound-induced Agglomeration. *New J. Chem.* **2002**, *26*, 416−420.

(17) Chen, X.; Mao, S. S. Titanium Dioxide Nanomaterials: Synthesis, Properties, Modifications, and Applications. *Chem. Rev.* **2007**, *107*, 2891−2959.

(18) Cargnello, M.; Gordon, T. R.; Murray, C. B. Solution-Phase Synthesis of Titanium Dioxide Nanoparticles and Nanocrystals. *Chem. Rev.* **2014**, DOI: 10.1021/cr500170p.

(19) Lazzeri, M.; Vittadini, A.; Selloni, A. Structure and Energetics of Stoichiometric TiO_2 Anatase Surfaces. *Phys. Rev. B* **2001**, *63*, 155409.

(20) Liu, M.; Piao, L.; Zhao, L.; Ju, S.; Yan, Z.; He, T.; Zhou, C.; Wang, W. Anatase TiO_2 Single Crystals with Exposed {001} and {110} Facets: Facile Synthesis and Enhanced Photocatalysis. *Chem. Commun.* **2010**, *46*, 1664−1666.

(21) Yang, H. G.; Liu, G.; Qiao, S. Z.; Sun, C. H.; Jin, Y. G.; Smith, S. C.; Zou, J.; Cheng, H. M.; Lu, G. Q. Solvothermal Synthesis and Photoreactivity of Anatase TiO_2 Nanosheets with Dominant {001} Facets. *J. Am. Chem. Soc.* **2009**, *131*, 4078−4083.

(22) Yang, H. G.; Sun, C. H.; Qiao, S. Z.; Zou, J.; Liu, G.; Smith, S. C.; Cheng, H. M.; Lu, G. Q. Anatase TiO_2 Single Crystals with a Large Percentage of Reactive Facets. *Nature* **2008**, *453*, 638−641.

(23) Fang, W. Q.; Gong, X.-Q.; Yang, H. G. On the Unusual Properties of Anatase TiO_2 Exposed by Highly Reactive Facets. *J. Phys. Chem. Lett.* **2011**, *2*, 725−734.

(24) Selloni, A. Anatase shows its Reactive Side. *Nat. Mater.* **2008**, *7*, 613−615.

(25) Pan, J.; Liu, G.; Lu, G. Q.; Cheng, H.-M. On the True Photoreactivity Order of {001}, {010}, and {101} Facets of Anatase TiO_2 Crystals. *Angew. Chem., Int. Ed. Engl.* **2011**, *50*, 2133−2137.

(26) Nguyen, C. K.; Cha, H. G.; Kang, Y. S. Axis-Oriented, Anatase TiO_2 Single Crystals with Dominant {001} and {100} Facets. *Cryst. Growth Des.* **2011**, *11*, 3947−3953.

(27) Han, X.; Wang, X.; Xie, S.; Kuang, Q.; Ouyang, J.; Xie, Z.; Zheng, L. Carbonate Ions-assisted Syntheses of Anatase TiO_2 Nanoparticles Exposed with High Energy (001) Facets. *RSC Adv.* **2012**, *2*, 3251−3253.

(28) Han, X.; Zheng, B.; Ouyang, J.; Wang, X.; Kuang, Q.; Jiang, Y.; Xie, Z.; Zheng, L. Control of Anatase TiO_2 Nanocrystals with a Series of High-Energy Crystal Facets via a Fuorine-Free Strategy. *Chem. − Asian J.* **2012**, *7*, 2538−2542.

(29) Dai, Y.; Cobley, C. M.; Zeng, J.; Sun, Y.; Xia, Y. Synthesis of Anatase TiO_2 Nanocrystals with Exposed {001} Facets. *Nano Lett.* **2009**, *9*, 2455−2459.

(30) Wu, B.; Guo, C.; Zheng, N.; Xie, Z.; Stucky, G. D. Nonaqueous Production of Nanostructured Anatase with High-Energy Facets. *J. Am. Chem. Soc.* **2008**, *130*, 17563−17567.

(31) Li, Y.-F.; Selloni, A. Theoretical Study of Interfacial Electron Transfer from Reduced Anatase TiO_2 (101) to Adsorbed O_2. *J. Am. Chem. Soc.* **2013**, *135*, 9195−9199.

(32) Tamaki, S.; Furube, A.; Murai, M.; Hara, K.; Katoh, R.; Tachiya, M. Direct Observation of Reactive Trapped Holes in TiO_2 Undergoing Photocatalytic Oxidation of Adsorbed Alcohols: Evaluation of the Reaction Rates and Yields. *J. Am. Chem. Soc.* **2006**, *128*, 416−417.

(33) Gottesman, R.; Tirosh, S.; Barad, H.-N.; Zaban, A. Direct Imaging of the Recombination/ Reduction Sites in Porous TiO_2 Electrodes. *J. Phys. Chem. Lett.* **2013**, *4*, 2822−2828.

(34) Roy, N.; Sohn, Y.; Pradhan, D. Synergy of Low-Energy {101} and High-Energy {001} TiO_2 Crystal Facets for Enhanced Photocatalysis. *ACS Nano* **2013**, *7*, 2532−2540.
(35) Tachikawa, T.; Yamashita, S.; Majima, T. Evidence for Crystal-Face-Dependent TiO_2 Photocatalysis from Single Molecule Imaging and Kinetic Analysis. *J. Am. Chem. Soc.* **2011**, *133*, 7197−7204.
(36) Maitani, M. M.; Tanaka, K.; Mochizuki, D.; Wada, Y. Enhancement of Photoexcited Charge Transfer by {001} Facet Dominating TiO_2 Nanoparticles. *J. Phys. Chem. Lett.* **2011**, *2*, 2655−2659.
(37) Burnside, S. D.; Shklover, V.; Barbe, C.; Comte, P.; Arendse, F.; Brooks, K.; Gratzel, M. Self-Organization of TiO_2 Nanoparticles in Thin Films. *Chem. Mater.* **1998**, *10*, 2419−2425.
(38) Wang, L.; Zang, L.; Zhao, J.; Wang, C. Green Synthesis of Shape-defined Anatase TiO_2 Nanocrystals wholly Exposed with {001} and {100} Facets. *Chem. Commun.* **2012**, *48*, 11736−11738.
(39) Xu, H.; Reunchan, P.; Ouyang, S.; Tong, H.; Umezawa, N.; Kako, T.; Ye, J. Anatase TiO_2 Single Crystals Exposed with High-Reactive {111} Facets Toward Efficient H_2 Evolution. *Chem. Mater.* **2013**, *25*, 405−411.
(40) Zhu, J.; Wang, S.; Bian, Z.; Xie, S.; Cai, C.; Wang, J.; Yangb, H.; Li, H. Solvothermally Controllable Synthesis of Anatase TiO_2 Nanocrystals with Dominant {001} Facets and Enhanced Photocatalytic Activity. *CrystEngComm.* **2010**, *12*, 2219−2224.
(41) Patra, A. K.; Dutta, A.; Bhaumik, A. Synthesis of Cuboid-Shaped Single-Crystalline TiO_2 Nanocrystals with High-Energy Facets {001} and Its Dye-Sensitized Solar Cell Application. *J. Phys. Chem. C* **2014**, *118*, 16703−16709.
(42) Tian, F.; Zhang, Y.; Zhang, J.; Pan, C. Raman Spectroscopy: A New Approach to Measure the Percentage of Anatase TiO_2 Exposed (001) Facets. *J. Phys. Chem. C* **2012**, *116*, 7515−7519.
(43) Balachandran, U.; Eror, N. G. Raman Spectra of Titanium Dioxide. *J. Solid State Chem.* **1982**, *42*, 276−282.
(44) Frank, O.; Zukalova, M.; Laskova, B.; Kurti, J.; Koltai, J.; Kavan, L. Raman Spectra of Titanium Dioxide (anatase, rutile) with Identified Oxygen Isotopes (16, 17, 18). *Phys. Chem. Chem. Phys.* **2012**, *14*, 14567−14572.
(45) Wang, Z.; Lv, K.; Wang, G.; Deng, K.; Tang, D. Study on the Shape Control and Photocatalytic Activity of High-energy Anatase Titania. *Appl. Catal., B* **2010**, *100*, 378−385.
(46) Lv, K.; Xiang, Q.; Yu, J. Effect of Calcination Temperature on Morphology and Photocatalytic Activity of Anatase TiO_2 Nanosheets with Exposed {001} Facets. *Appl. Catal., B* **2011**, *104*, 275−281.
(47) Dinh, C.-T.; Nguyen, T.-D.; Kleitz, F.; Do, T.-O. Shape-Controlled Synthesis of Highly Crystalline Titania NCs. *ACS Nano* **2009**, *11*, 3737−3743.
(48) Gong, X.-Q.; Selloni, A.; Batzill, M.; Diebold, U. Steps on Anatase TiO_2(101). *Nat. Mater.* **2006**, *5*, 665−670.
(49) Panaćek, A.; Prucek, R.; Hrbać, J.; Nevecnă, T.; Šteffkova, J.; Zboril, R.; Kvítek, L. Polyacrylate-Assisted Size Control of Silver Nanoparticles and Their Catalytic Activity. *Chem. Mater.* **2014**, *26*, 1332−1339.
(50) Houas, A.; Lachheb, H.; Ksibi, M.; Elaloui, E.; Guillard, C.; Herrmann, J.-M. Photocatalytic Degradation Pathway of Methylene Blue in Water. *Appl. Catal., B* **2001**, *3*, 1145−157.
(51) He, Y.; Grieser, F.; Ashokkumar, M. The Mechanism of Sonophotocatalytic Degradation of Methyl Orange and its Products in Aqueous Solutions. *Ultrason. Sonochem.* **2011**, *18*, 974−980.
(52) Baiocchi, C.; Brussino, M. C.; Pramauro, E.; Prevot, A. B.; Palmisano, L.; Marci, G. Characterization of Methyl Orange and its Photocatalytic Degradation Products by HPLC/UV−VIS Diode Array and Atmospheric Pressure Ionization Quadrupole Ion Trap Mass Spectrometry. *Int. J. Mass Spectrom.* **2002**, *214*, 247−256.
(53) Tong, T.; Zhang, J.; Tian, B.; Chen, F.; He, D. Preparation of Fe^{3+}-doped TiO_2 Catalysts by Controlled Hydrolysis of Titanium Alkoxide and Study on Their Photocatalytic Activity for Methyl Orange Degradation. *J. Hazard. Mater.* **2008**, *155*, 572−579.
(54) Kang, X.; Chen, S. Photocatalytic Reduction of Methylene Blue by TiO_2 Nanotube Arrays: Effects of TiO_2 Crystalline Phase. *J. Mater. Sci.* **2010**, *45*, 2696−2702.
(55) Galagan, Y.; Su, W.-F. Reversible Photoreduction of Methylene Blue in Acrylate Media Containing Benzyl Dimethyl Ketal. *J. Photochem. Photobiol., A* **2008**, *195*, 378−383.
(56) Tennakone, K.; Senadeera, S.; Priyadharshana, A. TiO_2 Catalyzed Photo-oxidation of Water in the Presence of Methylene Blue. *Sol. Energy Mater. Sol. Cells* **1993**, *29*, 109−113.
(57) Cong, Y.; Zhang, J.; Chen, F.; Anpo, M. Synthesis and Characterization of Nitrogen-Doped TiO_2 Nanophotocatalyst with High Visible Light Activity. *J. Phys. Chem. C* **2007**, *111*, 6976−6982.
(58) Lu, B.; Zhu, C.; Zhang, Z.; Lan, W.; Xie, E. Preparation of Highly Porous TiO_2 Nanotubes and their Catalytic Applications. *J. Mater. Chem.* **2012**, *22*, 1375−1379.
(59) Dawson, A.; Kamat, P. V. Semiconductor-Metal Nanocomposites. Photoinduced Fusion and Photocatalysis of Gold-Capped TiO_2 (TiO_2/Gold) Nanoparticles. *J. Phys. Chem. B* **2001**, *105*, 960−966.
(60) Li, H.; Bian, Z.; Zhu, J.; Huo, Y.; Li, H.; Lu, Y. Mesoporous Au/TiO_2 Nanocomposites with Enhanced Photocatalytic Activity. *J. Am. Chem. Soc.* **2007**, *129*, 4538−4539.
(61) Chen, X.; Burda, C. The Electronic Origin of the Visible-Light Absorption Properties of C-, N- and S-Doped TiO_2 Nanomaterials. *J. Am. Chem. Soc.* **2008**, *130*, 5018−5019.
(62) Laskova, B.; Zukalova, M.; Kavan, L.; Chou, A.; Liska, P.; Wei, Z.; Bin, L.; Kubat, P.; Ghadiri, E.; Moser, J. E.; Grätzel, M. Voltage Enhancement in Dye-sensitized Solar Cell using (001)-oriented Anatase TiO_2 Nanosheets. *J. Solid State Electrochem.* **2012**, *16*, 2993−3001.
(63) Bousa, M.; Laskova, B.; Zukalova, M.; Prochazka, J.; Chou, A.; Kavan, L. Polycrystalline TiO_2 Anatase with a Large Proportion of Crystal Facets (001): Lithium Insertion Electrochemistry. *J. Electrochem. Soc.* **2010**, *157*, A1108−A1112.
(64) Zhang, K.; Liu, Q.; Wang, H.; Zhang, R.; Wu, C.; Gong, J. R. TiO_2 Single Crystal with Four-Truncated-Bipyramid Morphology as an Efficient Photocatalyst for Hydrogen Production. *Small* **2013**, *9*, 2452−2459.
(65) Ma, X.; Dai, Y.; Guo, M.; Huang, B. Photooxidation and Photoreduction Activities of the {100}, {101}, and {001} Surfaces of Anatase TiO_2. *Langmuir* **2013**, *29*, 13647−13654.
(66) Wang, D.; Kanhere, P.; Li, M.; Tay, Q.; Tang, Y.; Huang, Y.; Sum, T. C.; Mathews, N.; Sritharan, T.; Chen, Z. Improving Photocatalytic H_2 Evolution of TiO_2 via Formation of {001}−{010} Quasi-Heterojunctions. *J. Phys. Chem. C* **2013**, *117*, 22894−22902.
(67) Nunzi, F.; Storchi, L.; Manca, M.; Giannuzzi, R.; Gigli, G.; Angelis, F. D. Shape and Morphology Effects on the Electronic Structure of TiO_2 Nanostructures: From Nanocrystals to Nanorods. *ACS Appl. Mater. Interfaces* **2014**, *6*, 2471−2478.